

An analytic function of lunar surface temperature for exospheric modeling



Dana M. Hurley^{a,*}, Menelaos Sarantos^{b,f}, Cesare Grava^c, Jean-Pierre Williams^d, Kurt D. Retherford^c, Matthew Siegler^e, Benjamin Greenhagen^e, David Paige^d

^a Johns Hopkins University Applied Physics Laboratory, Laurel, MD 20723, USA

^b Goddard Planetary Heliophysics Institute, University of Maryland Baltimore County, 21228, USA

^c Southwest Research Institute, San Antonio, TX 78228, USA

^d University of California, Los Angeles, CA 90095, USA

^e Jet Propulsion Laboratory, Pasadena, CA 91109, USA

^f Heliophysics Science Division, NASA Goddard Space Flight Center, Greenbelt, MD 20771, USA

ARTICLE INFO

Article history:

Received 28 May 2014

Revised 26 August 2014

Accepted 26 August 2014

Available online 6 September 2014

Keywords:

Moon, surface

Satellites, atmospheres

Atmospheres, structure

ABSTRACT

We present an analytic expression to represent the lunar surface temperature as a function of Sun-state latitude and local time. The approximation represents neither topographical features nor compositional effects and therefore does not change as a function of selenographic latitude and longitude. The function reproduces the surface temperature measured by Diviner to within ± 10 K at 72% of grid points for dayside solar zenith angles of $< 80^\circ$, and at 98% of grid points for nightside solar zenith angles $> 100^\circ$. The analytic function is least accurate at the terminator, where there is a strong gradient in the temperature, and the polar regions. Topographic features have a larger effect on the actual temperature near the terminator than at other solar zenith angles. For exospheric modeling the effects of topography on the thermal model can be approximated by using an effective longitude for determining the temperature. This effective longitude is randomly redistributed with 1 sigma of 4.5° . The resulting “roughened” analytical model well represents the statistical dispersion in the Diviner data and is expected to be generally useful for future models of lunar surface temperature, especially those implemented within exospheric simulations that address questions of volatile transport.

© 2014 Elsevier Inc. All rights reserved.

1. Introduction

The surface temperature is an important input to lunar exosphere models because it can modulate the velocity distribution of exospheric particles and adsorption of particles to the surface. Various approaches have previously been adopted to incorporate temperature variations across the surface in such models. Butler (1997) used a latitude function of temperature. Crider and Vondrak (2000) implemented a function of the solar zenith angle, where the nightside temperature was held constant. However, due to the finite thermal inertia of lunar regolith, a constant nighttime temperature is inconsistent with observations (Vasavada et al., 2012). It also fails to reproduce the nightside distribution of exospheric helium. To capture these effects Hodges (1973) used a linearly decreasing temperature on the lunar nightside from dusk to dawn to reproduce Lunar Atmospheric Composition Experiment (LACE) observations of helium. Leblanc and Chaufray (2011) also

reproduce the LACE results using a linear nightside temperature function, and further explore how choice of energy distribution and thermal accommodation factor influence the nightside helium density on the Moon.

More recently, the temperature of the surface of the Moon has been measured by the Diviner Lunar Radiometer Experiment (Diviner) onboard the Lunar Reconnaissance Orbiter (LRO) by mapping the albedo of the Moon through a range of IR wavelengths (Paige et al., 2010a). Diviner measures the albedo with 2 broadband solar channels. A further 7 narrowband channels spanning 7.55–400 μm wavelengths in the infrared provide brightness temperature data. As each channel will be affected by sub-pixel variations in the surface temperature differently, Paige et al. (2010b) defined a bolometric brightness temperature for describing the temperature of the lunar surface. Vasavada et al. (2012) used Diviner equatorial data to constrain a thermal model of the lunar regolith that includes a robust calculation of heat balance using model of regolith conductivity that exponentially increases as a function of depth.

* Corresponding author.

These global data can be deposited in a look-up table for implementation in models that require knowledge of the lunar surface temperature. Alternatively, a robust model such as Vasavada's can be used. However, exospheric models query the surface temperature many times as many test particles recycle on each simulation timestep, making it computationally intensive to use a look-up table for these types of simulations. There is a trade between runtime efficiency and accuracy in the temperature differences caused by composition, rock size, and topography. Thus an analytic function is advantageous in terms of ease of implementation and run-time efficiency. We present an analytic function for the surface temperature of the Moon that is only a function of position in Sun-state coordinates. The deviations of the analytic function from measured lunar temperature are presented for new Moon orientation. The function is a good representation of measured temperature, while neglecting effects tied to selenographic position.

2. Analytic function

The temperature function is an analytic approximation to the temperature observed by Diviner. It comprises two functions, one describing the day and one the night matched at the terminator. The observed dayside temperature is well-reproduced by a cosine function of the solar zenith angle, ψ , defined as the angle between the Moon–Sun line and the vector from the center of the Moon through the point on the lunar surface. Although the Lambertian model of dayside temperature calls for a function of $T_{ss} \cos^{1/4}(\psi)$, where T_{ss} is the subsolar temperature, this function goes to zero at the terminator, which is difficult to match to the nightside. Clementine long wave infrared (LWIR) data are consistent with the $\cos^{1/4}$ shape (Lawson et al., 2000) as are the dayside Diviner data (Vasavada et al., 2012). Leblanc and Chaufray (2011) assumed the dayside function to be in the form of:

$$T(\psi) = T_0 \cos^n(\psi) + T_1 \quad (\psi < 90^\circ) \quad (1)$$

which allows the temperature at the terminator to be defined, making it easier to implement in models. Dayside Diviner observations (Vasavada et al., 2012) are well reproduced using $T_0 = 262$ K, $T_1 = 130$ K, and $n = 1/2$. This function peaks at 392 K at the subsolar point and falls off slowly toward the terminator, where the temperature is 130 K:

$$T(\psi) = 262 \cos^{1/2}(\psi) + 130 \text{ K} \quad (\psi < 90^\circ) \quad (2)$$

An alternative is to use the $\cos^{1/4}(\psi)$ function but include a floor value that the calculated temperature is not allowed to be less than to ensure the value does not go below a preset limit at the terminator. We use:

$$T(\psi) = 392 \cos^{1/4}(\psi) > 130 \text{ K} \quad (\psi < 90^\circ) \quad (3)$$

which is more correct physically, but introduces a plateau within 1° SZA of the terminator that may not be desirable, depending on the application. This is problematic near the pole, where the function gives a constant dayside temperature at latitude within 1° of the pole.

We approximate the cooling of the nightside with a 6-term polynomial fit in longitude, φ . A latitude-dependence is also observed, and is reproduced using a sine function of the colatitude, θ . Using longitude (φ) in radians ranging from $(\pi/2, 3\pi/2)$ with $\varphi = \pi$ at midnight, the nightside temperature is approximated by:

$$T(\theta, \varphi) = \sum_{i=0, \dots, 5} (a_i \varphi^i) + 35(\sin(\theta) - 1) \quad (\psi > 90^\circ) \quad (4)$$

where $a = [444.738, -448.937, 239.668, -63.8844, 8.34064, -0.423502]$. At the equator, this function decreases from 130 K post-dusk to 95 K pre-dawn. There is a 35 K difference from the

equator to the pole at all longitudes. At high latitude, the function goes from 95 K at post-dusk to 60 K at pre-dawn. The pre-dawn polar region is the coldest location of the Moon using this analytic function. Fig. 1 (top) shows the temperature function using a $0.5^\circ \times 0.5^\circ$ resolution using Eq. (2) for the dayside and Eq. (4) for the nightside.

For comparison, Diviner data are shown (Fig. 1, middle). The Diviner maps are created from nadir-only Diviner level 1 data. Each data point is geometrically corrected using a Lunar Orbiter Laser Altimeter (LOLA) derived digital elevation map (DEM) defined on an icosahedral geodesic grid comprised of 83,886,080 triangles with sides ~ 1 km in length. Each data point is ray traced from the detector to the surface to determine the correct latitude and longitude that each observation was made. The data was then binned into 0.5° longitude and latitude bins and 0.25 h of local time. This procedure is done for each of the seven Diviner IR-channels, which are then used to determine the bolometric brightness temperature, the wavelength-integrated radiance expressed as a temperature of an equivalent blackbody (Paige et al., 2010b). This results in a diurnal temperature curve for each 0.5° map pixel with a temporal resolution of 0.25 h of local time. The temperature for each pixel, given a pixel's latitude, longitude, and local time relative to a subsolar point, is then interpolated from the pixel's 0.25 h binned diurnal curve to create maps of instantaneous global temperatures for any given subsolar point. The map in Fig. 1 uses the anti-Earth point as the subsolar point.

The relative difference in the analytic function and the data is shown (Fig. 1, bottom). At this resolution, 74% of the grid points are within ± 10 K of the Diviner observations. On the dayside at solar zenith angles $< 80^\circ$, 73% of grid points are within ± 10 K of the Diviner observations. The nightside function at solar zenith angles $> 100^\circ$ falls within ± 10 K for 98% of the gridpoints. The model values for locations within 10° of the lunar terminator deviate from the Diviner observations by less than ± 10 K on only 47% of the grid points. Thus, the function fits the Diviner observations well except near the terminator. The disagreement stems from the fact that temperature is an extremely strong function of incidence angle when the latter nears 90° (Vasavada et al., 2012). Topography at the terminator produces local variations in the incidence angle, which translates into large local variations in the temperature. Because the analytic function ignores topography, it cannot account for these effects.

In effect, the terminator is an inhomogeneous region for the lunar exosphere. In exospheric models, residence times of volatiles condensed on the nightside are a sensitive function of temperature in cooler locations and should be expected to vary widely at locations near the terminator. Therefore, the topographical effects will determine how far beyond the terminator the Moon must rotate to reach the release temperature for a given species. In addition, the vertical profile of exospheric density at the terminator may be sensitive to these shadowing effects because particles traversing the terminator were launched from a wide range of local temperatures.

This motivates a technique to implement an effective distribution that resembles the effect of topography without being tied to specific locations on the Moon. The surface temperature felt by a particle on contact with the surface can be calculated at a longitude shifted by a few degrees from the actual longitude of the point of contact. A simple method for this correction is to assign to each particle in the simulation an offset from the actual longitude for the purposes of calculating surface temperature using the analytical function $T(\theta, \varphi)$ defined previously. We suggest choosing an effective longitude from a Gaussian distribution of offset longitudes with a sigma of 4.5° . This distribution of effective longitudes is peaked on the actual longitude and includes small numbers of points with effective longitudes at further than $\pm 10^\circ$ from the actual longitude, representing thermal effects of sloped

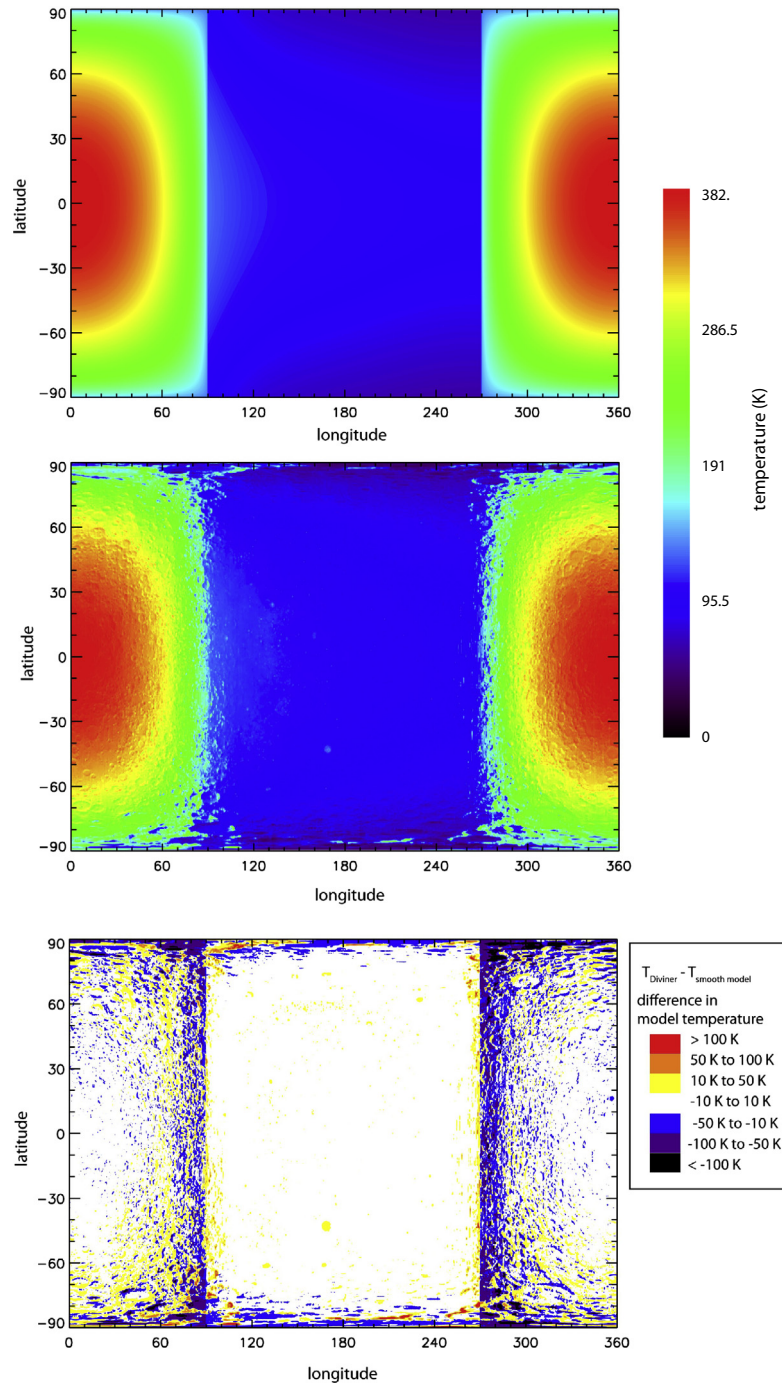


Fig. 1. (Top) The smooth analytic function of lunar surface temperature is shown in Sun-state coordinates as a function of latitude and eastern longitude, with $(0^\circ, 0^\circ)$ being the subsolar point, and longitude = 90° corresponds to dusk. (Middle) The Moon's surface temperature from Diviner data is shown. (Bottom) The comparison between the observation and analytic function is shown here as (Diviner map minus the smooth analytic function).

areas. Fig. 2 (top) shows the temperature using the Gaussian distribution of longitude offsets, hereafter called the roughened model. To compare with the Diviner map given in $0.5^\circ \times 0.5^\circ$ grid cells, this figure shows the temperature in the roughened model of one particle per grid cell. Although this method does not precisely reproduce any specific regions of the Moon, it produces the desired statistical effects on the particle scale heights and residence times necessary to accurately model the global lunar exosphere, especially at the high-temperature gradient across the terminators. The difference between the roughened model and smooth function is shown in Fig. 2 (bottom), analogous to the bottom of Fig. 1.

Perhaps a perturbation to the effective solar zenith angle would better reproduce the deviations at high latitude, but the longitude offset is very effective at the terminators. Alternatively, one could implement an additional offset function to latitude, although this has not been explored in this work.

We demonstrate how the implementation of roughness achieves the desired effects in exospheric modeling by calculating the local time of release of a set of argon atoms adsorbed to the nightside and comparing results using the roughened model to those using the Diviner map. The residence time and desorption probability are calculated using the function in Grava et al. (this

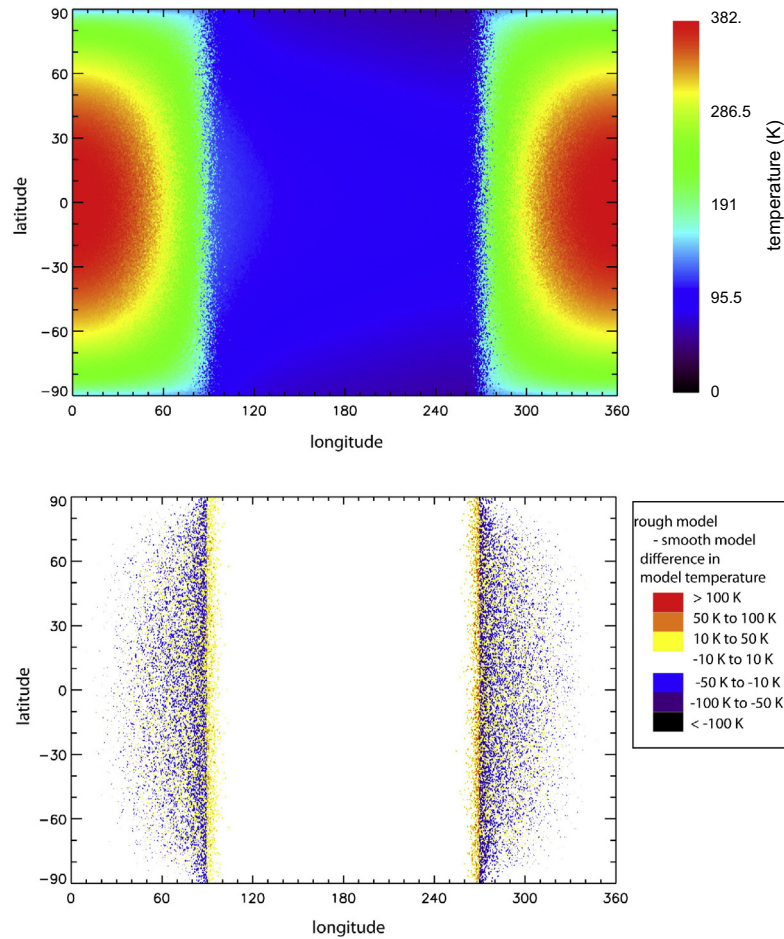


Fig. 2. The “roughened” model temperature is shown using the analytic function with a randomized perturbation to the longitude added to estimate effects from topography. A Gaussian distribution of longitudinal offsets with sigma 4.5° is added to the actual longitude for the longitude and solar zenith angle used to calculate the local surface temperature (top). The difference between the roughened model and the smooth model is shown (bottom) for comparison with the difference map in Fig. 1 (bottom).

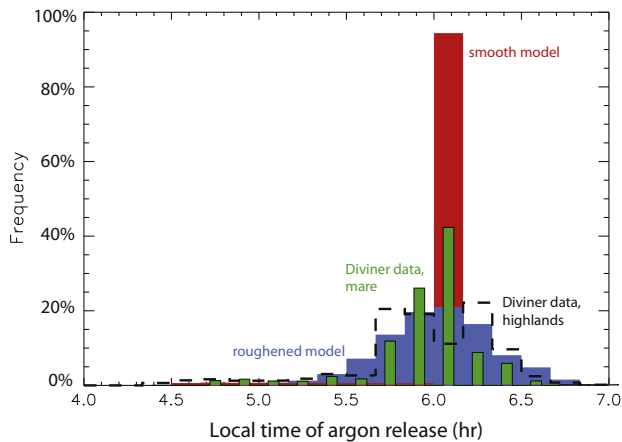


Fig. 3. The histogram shows the local time at which argon atoms desorb from the surface of the Moon in the model using the 3 different temperature functions: (black) Diviner data from a highlands region, (green) Diviner data from a mare region, (red) smooth analytic function, and (blue) roughened analytic function.

issue). One million argon atoms are distributed across all latitudes at 4:00 a.m. local time. The histogram depicting the local time at which they desorb in the model using Diviner data is shown in Fig. 3 in the black dashed line. There is a distribution in local release of atoms at about ± 30 min in local time about the dawn

terminator, i.e. 5:30–6:30 a.m. However, the smooth analytic model (red histogram) does not reproduce this distribution. Instead, almost all desorption occurs right at 6 a.m. Implementing the roughened model (blue) does a reasonably good job at reproducing the results using the Diviner temperatures.

3. Model approximations and over-simplifications

Seasonal effects have not been accounted for in this model. Thus it assumes that there is symmetry across the equator. Therefore the model will provide temperatures that are too high for the winter pole and too low for the summer pole.

The function neglects any effects of selenographic coordinates, thus treats maria and highlands the same. The higher albedo of the highland material reflects more sunlight, and is observed to be colder than the darker maria on the dayside of the Moon (Vasavada et al., 2012). In addition, there is a difference in the relative roughness of mare terrains from that of highlands terrains. Fig. 3 shows the difference in the local time of argon desorption when Diviner data are used from a highlands area (black line) and a mare area (green fill). The local time of desorption spans a narrower space for mare than highlands, related to the relative smoothness of the mare compared to the highlands. To account for this, one could implement a broader or narrower roughness function for a specific application to a particular terrain.

Also important to the lunar surface temperature is the rock abundance. Rocks have higher thermal inertia than fines, and are slower to warm on the dayside while retaining more heat on the nightside. The multispectral nature of the Diviner data enables decoupling of the contributions from rocks and fines and demonstrates that this is an observable effect on the Moon (Bandfield et al., 2011). However, it is necessarily neglected in the analytic function because including it would require tracking selenographic coordinates.

Similarly, this function does not include the extremely low temperatures found in permanently shadowed regions. The lowest measured temperatures on the Moon are found in permanently shadowed regions and range down to 25 K (Paige et al., 2010b). This is 20 K colder than the polar, pre-dawn temperature produced by the analytic function. However, as PSRs are tied to specific selenographic positions, they have been neglected in this formula for ease of application. Thus exospheric models that would examine the structure of the exosphere in the vicinity of cold traps should otherwise account for surface temperature in permanently shadowed regions. Historically, cold trapping over such regions has been treated probabilistically in such models by randomly removing a certain fraction of particles that impact within prescribed latitude bands (e.g., Butler, 1997; Grava et al., 2015).

The purpose of this function is to eliminate the need to query multiple lookup tables and interpolate between them as one would do if using Diviner data for the thermal information in the model. However, there are situations where it is more appropriate to use the Diviner data than the analytic model. For example, simulating data tied to a specific location on the surface of the Moon, like the LACE instrument, would be best accomplished by using the Diviner data at the Apollo 17 site and implementing a perturbation on that to represent small scale shadowing effects.

4. Conclusion

An analytic function of the lunar surface temperature that uses only position in Sun-state coordinates is presented for general ease of implementation of lunar surface temperature in models. The model is independent of selenographic position, and therefore neglects variations due to seasons, topography, rock abundance, and composition. Comparison with Diviner data indicates that the analytic function well represents the lunar surface temperature

over most of the Moon. The largest discrepancies occur within the permanently shadowed regions, which are neglected in the analytic function, and within $\pm 10^\circ$ of the lunar terminator, owing to the steep temperature gradient there which magnifies deviations from an assumed flat topography. The latter effect can be approximated by adding a randomly selected offset to the longitude for the purposes of calculating the surface temperature. A Gaussian distribution of offset longitudes with a sigma of 4.5° is folded into the analytical function to define an additional “roughened model”. Both the general and roughened analytical functions for lunar surface temperature presented in this work are expected to be useful for future investigations of lunar volatiles, with the roughened model especially well suited for studying exospheric transport processes.

Acknowledgments

This work was supported by the NASA Lunar Reconnaissance Orbiter project through the LAMP team. DMH thanks Rick Elphic and an anonymous referee for helpful suggestions.

References

- Bandfield, J.L., Ghent, R.R., Vasavada, A.R., Paige, D.A., Lawrence, S.J., Robinson, M.S., 2011. Lunar surface rock abundance and regolith fines temperatures derived from LRO Diviner Radiometer data. *J. Geophys. Res.* 116, E00H02.
- Butler, B., 1997. The migration of volatiles on the surfaces of Mercury and the Moon. *J. Geophys. Res.* 102 (E8), 19283–19291.
- Crider, D.H., Vondrak, R.R., 2000. The solar wind as a possible source of lunar polar hydrogen deposits. *J. Geophys. Res.* 105 (E11), 26773–26782.
- Grava, C., Chaufray, J.-Y., Retherford, K.D., Gladstone, G.R., Greathouse, T.K., Hurley, D.M., Hodges, R.R., Bayless, A.J., Cook, J.C., Stern, S.A., 2015. Lunar exosphere argon modeling. *Icarus* 255, 135–147.
- Hodges Jr., R.R., 1973. Helium and hydrogen in the lunar atmosphere. *J. Geophys. Res.* 78, 8055–8064.
- Lawson, S.L., Jakosky, B.M., Park, H.-S., Mellon, M.T., 2000. Brightness temperatures of the lunar surfaces: Calibration and global analysis of the Clementine long-wave infrared camera data. *J. Geophys. Res.* 105 (E2), 4273–4390.
- Leblanc, F., Chaufray, J.-Y., 2011. Mercury and Moon He exospheres: Analysis and modeling. *Icarus* 216, 551–559.
- Paige, D.A. et al., 2010a. The Lunar Reconnaissance Orbiter Diviner Lunar Radiometer Experiment. *Space Sci. Rev.* 150 (1–4), 125–160.
- Paige, D.A. et al., 2010b. Diviner Lunar Radiometer observations of cold traps in the Moon's south polar region. *Science* 330 (6003), 479–482.
- Vasavada, A.R., Bandfield, J.L., Greenhagen, B.T., Hayne, P.O., Siegler, M.A., Williams, J.-P., Paige, D.A., 2012. Lunar equatorial surface temperatures and regolith properties from the Diviner Lunar Radiometer experiment. *J. Geophys. Res.* 117, E00H18.